

Neural Plasticity-Inspired Multimodal Foundation Model for Earth Observation

Zhitong Xiong¹, Yi Wang¹, Fahong Zhang¹, Adam J. Stewart¹,
Joëlle Hanna², Damian Borth², Ioannis Papoutsis³,
Bertrand Le Saux⁴, Gustau Camps-Valls⁵, Xiao Xiang Zhu^{1,6*}

¹Chair of Data Science in Earth Observation, Technical University of
Munich (TUM), Arcisstraße 21, 80333 Munich, Germany.

²AIML Lab, School of Computer Science, University of St. Gallen,
Rosenbergstrasse 30, 9000 St. Gallen, Switzerland.

³School of Rural, Surveying and Geoinformatics Engineering, National
Technical University of Athens, Zografou 157 73, Greece.

⁴ESRIN, Φ-lab, European Space Agency (ESA), 00044 Frascati, Italy.

⁵Image Processing Laboratory (IPL), Universitat de València, Cat.
Agustín Escardino Benlloch 9, 46980 Paterna, València, Spain.

⁶Munich Center for Machine Learning, 80333 Munich, Germany.

*Corresponding author(s). E-mail(s): xiaoxiang.zhu@tum.de;

Abstract

The development of foundation models has revolutionized our ability to interpret the Earth’s surface using satellite observational data. Traditional models have been siloed, tailored to specific sensors or data types like optical, radar, and hyperspectral, each with unique characteristics. This specialization hinders the potential for a holistic analysis that could benefit from the combined strengths of these diverse data sources. Our approach introduces the Dynamic One-For-All (DOFA) model, leveraging the concept of neural plasticity in brain science to integrate various data modalities into a single framework adaptively. This dynamic hypernetwork, adjusting to different wavelengths, enables a single versatile Transformer jointly trained on data from five sensors to excel across 14 distinct Earth observation tasks, including sensors never seen during pretraining. DOFA’s innovative design offers a promising leap toward more accurate, efficient, and unified Earth observation analysis, showcasing remarkable adaptability and performance in harnessing the potential of multimodal Earth observation data.

Earth observation (EO) through satellite remote sensing rapidly enables deeper modeling and understanding of the Earth system¹⁻³. This pursuit is supported by the increasing deployment of satellites and sensors, each designed to capture distinct aspects of the Earth’s surface at varied spatial, spectral, and temporal resolutions. The advancement in observational technologies has unleashed a deluge of data surpassing hundreds of petabytes across the atmosphere, ocean, land, and cryosphere, offering unprecedented insights into various physical and biological processes. The data from such diverse missions as Landsat⁴, Sentinels⁵, MODIS⁶, EnMAP⁷, Gaofen⁸, and NAIP⁹ presents a rich yet complex mosaic of the Earth’s surface. Interpreting the multifaceted EO data through artificial intelligence can unlock remarkable possibilities for understanding complex environmental processes, from climate monitoring to disaster response and sustainable development¹⁰⁻¹². Traditional deep learning models utilize annotated datasets from these diverse data sources to train task-specific models². However, this paradigm necessitates substantial human efforts in dataset collection and annotation, alongside significant computational resources for model training and evaluation. In response to these challenges, foundation models (FMs)¹³, generally trained on broad data, have gained traction and popularity. Notable examples of foundation models encompass large language models like LLaMA¹⁴, GPT-3¹⁵, and ChatGPT¹⁶, as well as prominent visual models such as CLIP¹⁷, BLIP¹⁸, and SAM¹⁹. The essential advantage of such models is their ability to be adapted for specific downstream tasks with relatively fewer annotated data points, benefiting from the general feature representations learned from massive unlabelled data.

One of the key challenges in developing EO foundation models is coping with multi-sensor data. Earlier methods were typically designed to specialize in a single data source or a specific range of spatial and spectral resolutions. For example, existing pre-trained models like GFM²⁰, Scale-MAE²¹, and Cross-scale-MAE²² are pretrained for optical data. FG-MAE²³ and SatMAE²⁴ are developed for multi-spectral Sentinel-2 data, while SSL4EO-L²⁵ is designed for image data from Landsat. CROMA²⁶ designs two unimodal encoders to encode multi-spectral and synthetic aperture radar (SAR) data. A cross-modal radar-optical transformer is utilized to learn unified deep representations. DeCUR²⁷ is a bimodal self-supervised model that decouples the unique and common representations between two different modalities. SpectralGPT²⁸ is a foundation model tailored for multispectral remote sensing data. Additionally, Satlas²⁹ comprises a large-scale dataset from various sensors, with individual pretrained models provided for each sensor.

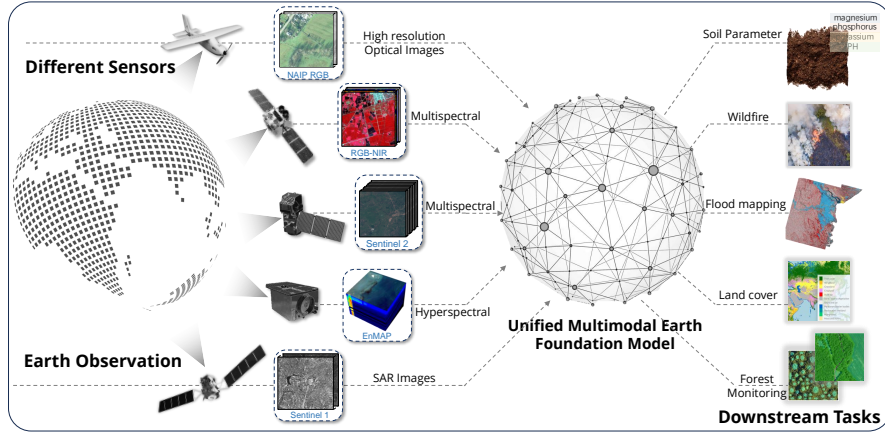
Current FMs for processing EO data often fall short of harnessing the full spectrum of information available, as they tend to focus narrowly on a single sensor modality or use distinct vision encoders for each type of sensor data. This strategy, while functional, does not tap into the vast potential offered by the optimum fusion of complementary information provided by multimodal data. Moreover, a critical limitation of these existing approaches is their lack of flexibility when adapting to diverse downstream tasks, which deviates from the original intent of designing FMs. In this regard, both the development of separate FMs and the extraction of multi-sensor features using separate visual encoders fail to account for this inter-sensor relationship, leading to the following limitations:

- The learned multimodal representation may not effectively capture such an inter-sensor relationship.
- The performance of foundation models will degrade when downstream tasks require the utilization of data from unseen sensors with varying numbers of spectral bands and spatial resolutions or different wavelength regimes.
- The development of individual, customized foundation models requires considerably more computing resources and human effort.
- The increasing number of specialized foundation models makes it difficult to select the most appropriate one for a specific downstream task.

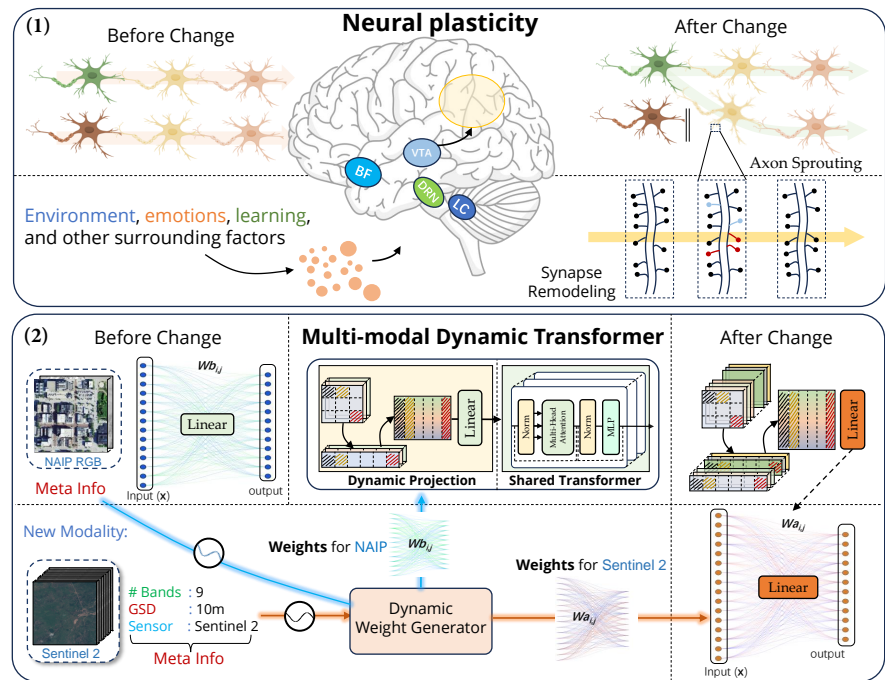
We aim to address these limitations and develop versatile FMs capable of adaptively processing this wide array of EO data, as illustrated in Fig. 1a. Specifically, we propose to build an adaptive foundation model to overcome the inefficiencies and complexities of employing separate vision encoders for each data type. To this end, we draw inspiration from the concept of neuroplasticity in neuroscience^{30–34}. Neuroplasticity embodies the dynamic ability of the brain to reorganize and adapt its neural connections in response to varying stimuli, experiences, and environmental changes. As shown in Fig. 1b (1), axon sprouting³⁵ and synapse remodeling³⁶ are two different types of neuroplasticity. It is an essential brain mechanism for adjusting to new experiences or environmental shifts³⁷. Drawing inspiration from this concept, we propose a **D**ynamic **O**ne-**F**or-**A**ll model (DOFA), designed to emulate a dynamic mechanism for processing multimodal EO data. As shown in Fig. 1b (2), DOFA is designed to adaptively alter its network weights in response to novel data modalities³⁸.

DOFA employs an innovative approach utilizing wavelength as a unifying parameter across various EO modalities to achieve a more cohesive multimodal representation. At its core, the model integrates a hypernetwork³⁹ that dynamically generates network weights based on the central wavelengths of each spectral band. This dynamic weight generator adjusts network weights to align with the specific modality of the input data, facilitating a customized network for each modality. Additionally, DOFA integrates a shared vision backbone, acting as a universal feature learning module for all heterogeneous data modalities. This framework enhances the model’s capacity to learn shared representations across diverse modalities. DOFA is trained using a masked image modeling strategy, including a distillation loss to optimize its performance further. This strategy facilitates quicker model convergence to reduce computational costs and enhances model performance by leveraging powerful representations from models pretrained on the ImageNet dataset⁴⁰.

In the evaluation phase, we thoroughly test DOFA on diverse real-world tasks, showing that it surpasses current leading foundation models in most downstream (13 out of 14) datasets. This performance, achieved with a singular network using identical pretraining, underscores DOFA’s superior handling of multimodal EO data. DOFA mirrors the dynamic learning of the human brain for continuous model improvement from diverse data sources, making it highly adaptable for the broad data spectrum in remote sensing. The experimental results showcase DOFA’s versatility and effectiveness and confirm DOFA as a novel foundation model for analyzing complex remote sensing data. Although DOFA is proposed for analyzing EO data, its methodology can



(a)



(b)

Fig. 1: Motivation and main architecture of DOFA. (a) Our primary purpose is to develop versatile foundation models capable of adaptively processing various EO data modalities. (b) We design DOFA to emulate the Neuroplasticity^{30–32} mechanism for processing multimodal EO data. (1) Illustration of axon sprouting and synapse remodeling. These two types of neuroplasticity represent the brain’s capability to adapt its structure and function to learned information, experience, or injury. (2) Illustration of the core idea of DOFA. DOFA is designed to adaptively alter its network weights in response to novel data modalities.

be widely applied to other domains where multimodal data is the mainstream such as medical image analysis, robotics, and climate modeling.

Results

In this section, we introduce the core concept of the DOFA framework. We then demonstrate how DOFA, utilizing identical pre-trained weights, exhibits robust generalization across a variety of EO downstream tasks with different data modalities. We evaluate DOFA’s performance through three experimental settings: linear probing across six classification datasets, partial fine-tuning across six segmentation datasets, and full fine-tuning on two downstream datasets (Supplementary Material E). These datasets span key EO applications, involving both image-level classification and pixel-level semantic segmentation tasks. Typically, existing FMs are confined to a fixed number of input channels, restricted by network architecture constraints. In contrast, DOFA’s design, inspired by neuroplasticity, enables adaptation to various data modalities, including previously unseen ones. Beyond its adaptability, DOFA consistently outperforms specialized FMs tailored for specific modalities. The superior performance of DOFA across these diverse datasets underscores its effectiveness, versatility, and capacity to generalize to novel sensors.

DOFA framework

Overview of DOFA. DOFA is a foundation model architecture that builds on the principles of masked image modeling, introducing a significant advancement by processing input images with any number of channels. This is enabled by the designed hypernetwork-based dynamic weight generator, which adapts to the spectral wavelength of each channel. By embedding images with varying channel numbers into a unified feature space, the model leverages shared Transformer networks to learn modality-shared representations. This architecture enables the model to learn versatile multimodal representations and handle diverse data modalities within a single framework. In summary, DOFA consists of four parts: 1) wavelength-conditioned dynamic patch embedding; 2) multimodal pre-training with shared Transformer networks; 3) masked image modeling with a variable number of spectral bands; and 4) distillation-based multimodal continual learning. Each of these parts is described below. An illustration of the overall architecture and more model details are provided in the Methods section.

Wavelength-conditioned dynamic patch embedding. We propose to utilize wavelength as a unifying parameter across various EO modalities to achieve uniform multimodal representations. Specifically, we project the data into the same feature dimensionality using the wavelength-conditioned dynamic patch embedding layer \mathcal{F}_{dpe} . Given the wavelengths $\lambda \in \mathbb{R}^C$ of a C -channel image, the hyper-network \mathcal{F}_{dpe} takes λ as input and outputs weights \mathbf{M}_w and biases \mathbf{M}_b . This can be formulated as $(\mathbf{M}_w, \mathbf{M}_b) = \mathcal{F}_{dpe}(\lambda)$. Then the generated \mathbf{M}_w and \mathbf{M}_b can be used as the parameters of the dynamic patch embedding layer.

Multimodal pre-training with shared Transformer networks. DOFA seeks to employ a unified network architecture to learn deep representations across diverse

data modalities. To achieve this, DOFA utilizes a shared vision Transformer backbone, which serves as a universal feature learning module for all heterogeneous data types. This approach compels the model to identify and learn common features across different modalities, fostering more versatile and robust representation learning.

Masked image modeling with any number of spectral bands. DOFA is trained based on the masked image modeling strategy, utilizing a masked auto-encoder architecture to reconstruct input data with different numbers of spectral bands. To this end, a wavelength-conditioned dynamic decoder layer is designed. This layer functions in concert with the wavelength-conditioned dynamic patch embedding layer, sharing a similar computational process. By integrating these dynamic layers, DOFA can perform masked reconstruction tasks on input data with an arbitrary number of spectral bands, enabling the training across different imaging modalities.

Distillation-based multimodal continual pretraining. Pre-training on massive datasets across multiple data modalities incurs significant computational costs. Towards carbon-minimized pre-training, we propose a distillation loss strategy to optimize DOFA across various data modalities. This approach enables efficient knowledge transfer and reduces the environmental impact of training large-scale models by leveraging representations from models pretrained on the ImageNet dataset.

Experimental settings

An effective unified multimodal foundation model would offer pretrained weights well characterizing the underlying training data, lead to excellent performances on a wide range of downstream tasks and datasets compared to existing state-of-the-art (SOTA) FMs after fine-tuning, and outperform individual FMs trained on a single modality. To comprehensively evaluate DOFA, we adopt three strategies for adapting it to downstream tasks. The first is linear probing, where only the added linear layers are trainable and the backbone network remains fixed. In this setting, we adopt six classification datasets from Geo-Bench⁴¹ for model evaluation and comparison. Geo-Bench serves as an excellent benchmark for evaluating and comparing EO foundation models due to its carefully curated datasets and extensive range of EO applications. The second strategy is partial fine-tuning, where the backbone is fixed and the other parts of the model are trainable. In this setting, six segmentation datasets from Geo-Bench are adopted for model evaluation. The third strategy is full fine-tuning, in which all parameters are learnable during the fine-tuning process. In this setting, the RESISC-45 and SegMunich datasets are utilized for model evaluation. To comprehensively demonstrate DOFA’s effectiveness and generalizability, these datasets cover both image-level classification and pixel-level semantic segmentation tasks. Detailed descriptions of the downstream datasets are available in Supplementary Material C.

Compared to other FMs, DOFA excels in handling data with variable numbers of spectral bands. Thus, we can adapt DOFA to 14 distinct downstream tasks with a single set of pre-trained weights. In some cases, existing FMs, such as GFM, Scale-MAE, and Cross-scale MAE, that are pretrained with RGB data, fail to adapt to datasets utilizing multispectral data directly. Regarding the pre-training weights, the evaluation settings for DOFA and other existing FMs can be summarized as follows:

1. Since DOFA can handle any number of spectral bands, it can be adapted to all the downstream datasets, even to unseen sensors. Thus, DOFA is pretrained on the curated multimodal dataset and uses the same parameters across all downstream tasks.
2. Most existing FMs, limited by their network architecture, cannot be adapted to data modalities different from those they were pretrained on. Thus, existing methods are pretrained on a specific modality and evaluated on downstream tasks within the same modality.

To comprehensively analyze the proposed model’s performance, we organized our experiments as follows:

- We showcase the performance of using fully-supervised training with ImageNet pretrained weights on the GEO-Bench⁴¹ datasets. This comparison highlights the energy efficiency of foundation models when achieving comparable or superior performance to fully supervised models.
- To demonstrate the value of using pretrained weights, we provide linear probing results from the ViT model initialized with random weights.
- We present results from models trained exclusively on a single data modality to highlight the benefits of leveraging multiple data modalities.
- We compare DOFA with existing SOTA foundation models that provide pretrained model weights, including Scale-MAE²¹, GFM²⁰, Cross-Scale MAE²², CROMA²⁶, FG-MAE²³, OFA-Net⁴², and SpectralGPT²⁸.
- We conduct full fine-tuning experiments on the RESISC-45 and the SegMunich datasets to compare with existing SOTA foundation models.

Note that, for linear probing, all models are trained for 50 epochs with only one linear layer trainable in the transfer learning setting. For partial fine-tuning, only the parameters in the segmentation head are trained for 20 epochs. For the fine-tuning experiments, all parameters of the models are trained with sufficient epochs until convergence. Supplementary Materials A, B, and D provide more detailed information about the compared models and DOFA implementation.

DOFA masters arbitrary classification tasks

The results on six classification downstream tasks are presented in Table 1. “Fully Trained” denotes the models using ImageNet pretrained weights for transfer learning and fully training the model on each dataset individually. We report the results of three different backbones on the GEO-Bench dataset: ViT-S⁴⁴, SwinV2-T⁴⁵, and ConvNext-B⁴⁶.

Although these models can perform better than self-supervised learning models in the linear probing setting, they entail significantly higher cost, time, and energy training expenses. Moreover, adapting each distinct network architecture to various datasets demands substantial efforts in hyper-parameter tuning. In contrast, pre-trained weights can save training costs and time. Merely 50 epochs of linear probing with pretrained weights can yield performance comparable to fully trained models, highlighting the advantage of EO foundation models.

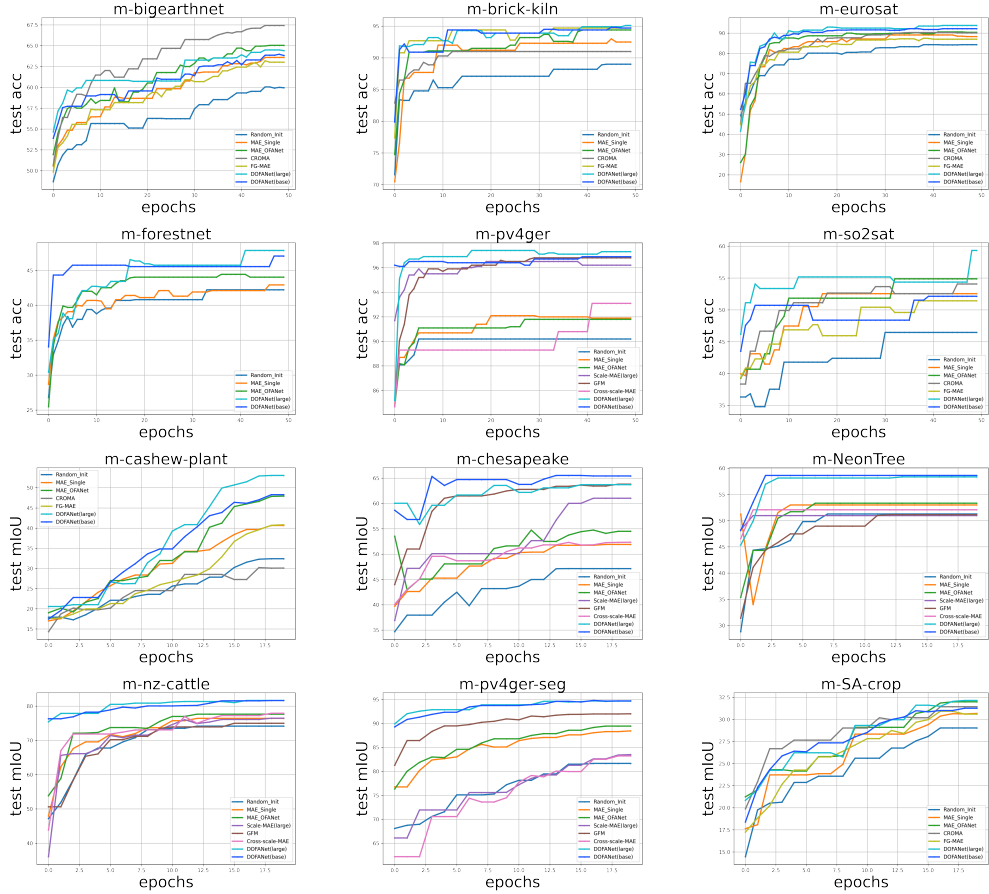
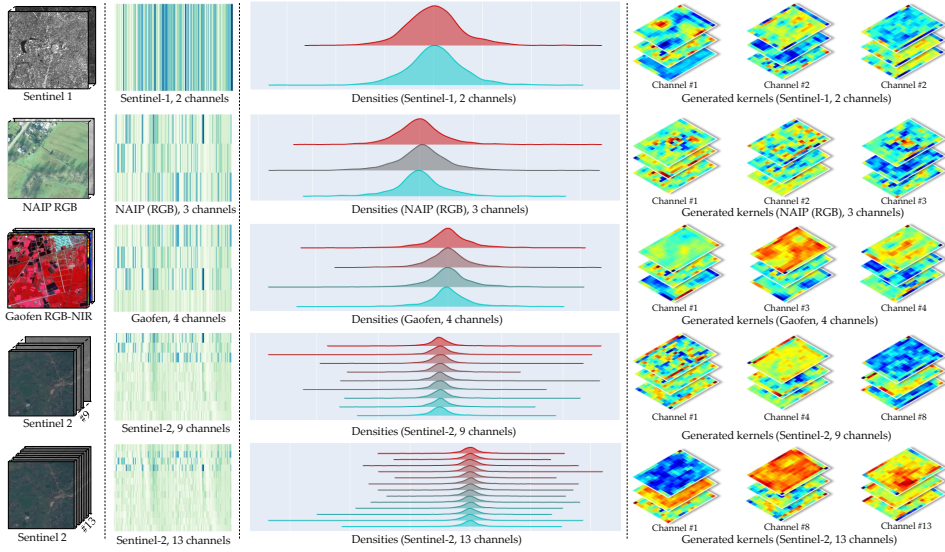
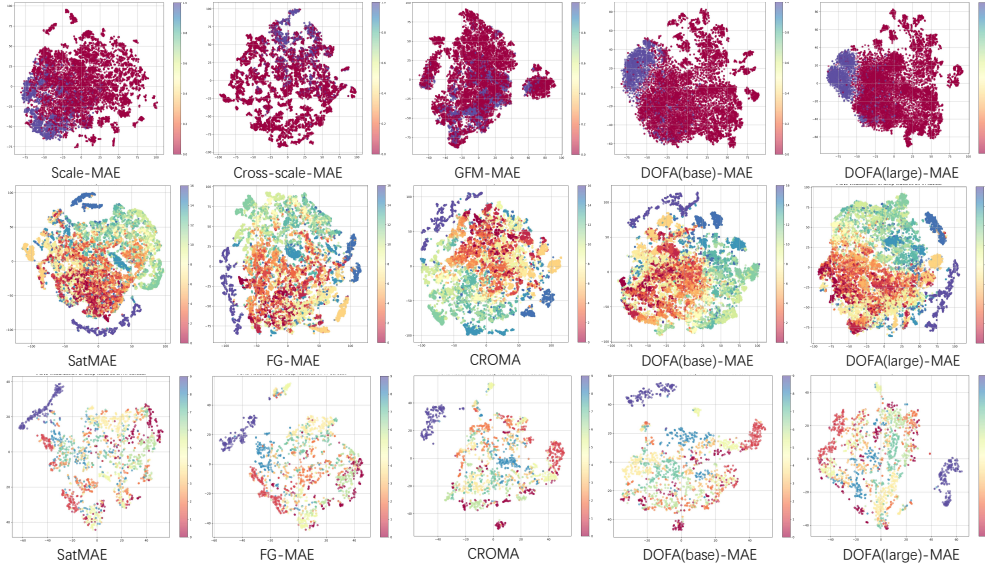


Fig. 2: Accuracy curves for various foundation models. All results are for fine-tuning experiments on the GEO-Bench dataset. Rows 1 and 2: Top-1 accuracy for classification datasets. Rows 3 and 4: Mean intersection over union (mIoU) for segmentation datasets. It can be seen that DOFA converges faster and achieves better performance than other models on most datasets.

We compare seven different SOTA self-supervised models. It can be seen that the data from other datasets has diverse spectral bands. Aside from the proposed DOFA, no existing model is universally adaptable for all downstream tasks in the transfer learning setting. For example, the “m-forest” dataset contains images from Landsat 8, which differs from all the data modalities used to train the compared models. However, in this case, the proposed DOFA can still be used for linear probing, even though it has never seen Landsat imagery during pre-training. This demonstrates that foundation models individually developed for a single modality have limitations when applied to real-world EO applications. DOFA is flexible enough to apply to all EO data modalities.



(a) **Visualization of the dynamic weight generator.** From left to right: examples of input images, learned embeddings for different central wavelengths, the histogram distributions of the generated weights, and some examples of the generated kernel weights.



(b) **t-SNE plots of the feature representations from various foundation models across multiple datasets.** From top to bottom row: the m-pv4ger dataset, the m-so2sat dataset, and the m-eurosat dataset. Enhanced separability signifies more effective representations.

Fig. 3: Visualization of learned embeddings. (a) Visualization of the generated weights for different input modalities. (b) t-SNE plots of the feature representations from various foundation models across multiple datasets.

Table 1: Linear probing results on six classification tasks. All models are trained for 50 epochs. The reported numbers are top-1 overall accuracy (OA). Missing values are due to the inability of the model to adapt to this domain.

Method	Backbone	m-bigearthnet	m-forestnet	m-brick-kiln	m-pv4ger	m-so2sat	m-entrosat
Fully Trained	ViT-S	66.0	53.8	98.1	97.6	57.5	97.3
Fully Trained	SwinV2-T	70.0	58.0	98.7	98.0	56.1	97.4
Fully Trained	ConvNext-B	69.1	56.8	98.9	98.0	58.1	97.7
rand. init.	ViT-B	52.9	41.5	84.5	91.3	38.3	85.7
MAE.Single ⁴³	ViT-B	63.6	-	88.9	92.2	50.0	89.0
OFA-Net ⁴²	ViT-B	65.0	-	94.7	93.2	49.4	91.9
SatMAE ²⁴	ViT-B	62.1	-	93.9	-	46.9	86.4
Scale-MAE ²¹	ViT-L	-	-	-	96.9	-	-
GFM ²⁰	Swin-B	-	-	-	96.8	-	-
Cross-Scale MAE ²²	ViT-B	-	-	-	93.1	-	-
FG-MAE ²³	ViT-B	63.0	-	94.7	-	51.4	87.0
CROMA ²⁶	ViT-B	67.4	-	91.0	-	49.2	90.1
DOFA	ViT-B	63.8	45.3	94.7	96.9	52.1	92.2
DOFA	ViT-L	64.4	47.4	95.1	97.3	59.3	93.8

Table 2: Partial fine-tuning results on six segmentation tasks. All models are trained with a frozen backbone for 20 epochs. Reported numbers are mean intersection over union (mIoU). Missing values are due to the inability of the model to adapt to this domain.

Method	Backbone	m-pv4ger-seg	m-nr-cattle	m-NeonTree	m-cashew-plant	m-SA-crop	m-chesapeake
DeepLabv3	ResNet101	93.4	67.6	53.9	48.6	30.4	62.1
U-Net	ResNet101	94.1	80.5	56.6	46.6	29.9	70.8
rand. init.	ViT-B	81.7	74.1	51.7	32.4	29.0	47.1
MAE.Single ⁴³	ViT-B	88.4	76.4	53.0	40.7	30.7	51.9
OFA-Net ⁴²	ViT-B	89.4	77.6	53.3	47.9	31.9	54.5
Scale-MAE ²¹	ViT-L	83.5	76.5	51.0	-	-	61.0
GFM ²⁰	Swin-B	92.0	75.0	51.1	-	-	63.8
Cross-Scale MAE ²²	ViT-B	83.2	77.9	52.1	-	-	52.3
CROMA ²⁶	ViT-B	-	-	-	30.1	31.4	-
FG-MAE ²³	ViT-B	-	-	-	40.8	30.6	-
DOFA	ViT-B	94.7	81.6	58.6	48.3	31.3	65.4
DOFA	ViT-L	95.0	81.7	59.1	53.8	32.1	66.3

Regarding performance, DOFA obtains the best results on all datasets except the “m-bigearthnet” dataset. DOFA uses a single pretrained model without switching to different pretrained weights or network architectures. This indicates that DOFA transfers to different downstream tasks effectively, even for new sensors (Landsat 8). This comparison with fully supervised training results highlights that foundation models,

with minimal and energy-efficient fine-tuning, can achieve comparable or superior performance to that of extensively supervised trained models. On the “m-bigearthnet” dataset, although the performance is not the best, it is still competitive compared with other SOTA models. Notably, on the “m-so2sat” dataset, DOFA with ViT-Large backbone achieves a top-1 overall accuracy of 59.3%, even higher than the fully trained models. The comparison results reveal that DOFA, designed to serve a general purpose, is a promising EO foundation model that can be effective in various downstream tasks.

We visualize the accuracy curves of different SOTA models in Fig. 2 for the classification and segmentation datasets. These figures show that the proposed DOFA converges faster than other models and performs better on most datasets.

In the full fine-tuning setting, DOFA is benchmarked against existing models such as Scale-MAE and SatMAE on the image classification dataset RESISC45, as presented in the Extended Table S1. Even utilizing the ViT-Base version, DOFA significantly outperforms the other methods. This performance underscores the effectiveness of the wavelength-conditioned dynamic patch embedding and the multimodal Transformer layers, demonstrating robust results when fine-tuned on downstream tasks. Utilizing the ViT-Large version, DOFA sets new SOTA performance on this dataset. Additionally, in the linear probing (frozen) setting, DOFA largely surpasses existing models, indicating its ability to adapt to downstream applications quickly.

DOFA outperforms single-source models for segmentation tasks

The results on six segmentation tasks are displayed in Table 2. For the segmentation tasks, we compare two types of models. One is a fully-trained model using the ResNet101 backbone and pretrained weights on ImageNet. In the other type, each model is pretrained using self-supervised methods. For these models, we freeze the weights of their backbone and only fine-tune the segmentation head. To ensure a fair comparison, UPerNet⁴⁷ is used for all these models as the segmentation head. The results show that DOFA performs even better than the fully trained DeepLabv3 and U-Net models. Note that DOFA models only train the segmentation head for 20 epochs, which is fast and energy-efficient. Compared with other foundation models, the results of DOFA with ViT-Base and ViT-Large backbones show clear superiority, especially on the “m-NeonTree” and the “m-nz-cattle” datasets. The performance across six segmentation tasks further validates DOFA’s versatility as an EO foundation model, which can support both classification and segmentation downstream tasks.

Similarly, we visualize the accuracy curves of different models in Fig. 2 for these six segmentation datasets. Observations indicate that DOFA achieves superior accuracy and faster convergence than other SOTA models. Overall, performance on these six datasets reveals DOFA’s versatility, effectiveness, and robust applicability across diverse downstream tasks.

In the full fine-tuning setting, we evaluate DOFA on the SegMunich dataset to compare it with existing SOTA models like SpectralGPT and SatMAE on semantic segmentation tasks. The results are presented in the Extended Table S2, demonstrating that the ViT-Base version of DOFA can outperform existing models tailored for

the Sentinel-2 modality. This indicates that the learned multimodal representation in DOFA works well when fine-tuned in segmentation tasks.

Visual Understanding of DOFA

DOFA generates diverse weights dynamically. We visualize the learned embeddings of various wavelengths and the generated kernels for different sensors in Fig. 3a for a better understanding of DOFA. We randomly select and plot six 16×16 kernel weights for input images with more than four channels. The figures indicate that DOFA can generate weights for different sensors dynamically and effectively.

DOFA optimizes separability in latent space. We visualize the pretrained representations of different models using the dimensionality reduction technique t-SNE⁴⁸ to represent high-dimensional data. Specifically, the extracted features of the pretrained models on downstream datasets m-pv4ger, m-so2sat, and m-eurosat are shown in Fig. 3b. Different colors represent different semantic categories. On these three datasets, the learned features of both versions of DOFA are clustered better than those of other compared models. These figures further validate the effectiveness of the proposed DOFA as a unified EO foundation model.

Discussion

In this work, we present a multimodal foundation model, inspired by neural plasticity. This innovative “dynamic one-for-all” framework is designed to handle an extensive variety of data types, modalities, and spatial resolutions. Emulating the human brain’s adaptability, it processes diverse data modalities with unprecedented versatility and efficiency. The proposed DOFA successfully demonstrates the enhanced utility and effectiveness of foundation models for diverse downstream tasks. This achievement underscores the potential of our dynamic model to revolutionize the way we interpret and analyze Earth’s spatial data.

While we have achieved significant milestones, challenges persist in refining the model’s performance across different data modalities, particularly through the advancement of multimodal pre-training techniques. The future presents expansive opportunities for DOFA, and the potential to extend its applications across a wider spectrum of data types and tasks and incorporate more varied data modalities such as LiDAR point clouds and textual data. Future iterations of DOFA will prioritize integrating diverse data modalities, including time-series data, to enhance the understanding of Earth’s dynamics. This unified approach aims to revolutionize applications in Earth system modeling and weather and climate analysis by providing a comprehensive view of environmental processes.

Methods

Here, we provide detailed information about the proposed DOFA model and a more detailed presentation of the training method.

Mathematical formalism

Given an input image $\mathbf{X} \in \mathbb{R}^{C \times H \times W}$, where H , W , and C represent the height, width, and number of channels, respectively, the image is first divided into a patch sequence. Each patch has a fixed spatial size $P \times P$ with C channels, and thus the image is converted into $N = \frac{HW}{P^2}$ patches. Each patch is flattened into a vector and linearly transformed into a D -dimensional embedding. This transformation is represented by a trainable embedding matrix $\mathbf{E} \in \mathbb{R}^{P^2 C \times D}$.

Formally, the patch embedding can be described as

$$\mathbf{X} = [\mathbf{X}_{p_1}; \mathbf{X}_{p_2}; \dots; \mathbf{X}_{p_N}], \quad \mathbf{X}_{p_i} \in \mathbb{R}^{P^2 C}, \quad (1)$$

where \mathbf{X}_{p_i} is the flattened vector of the i -th patch. Next, the flattened vectors are linearly projected into D -dimensional embeddings with a learnable embedding matrix:

$$\mathbf{Z}_0 = [\mathbf{X}_{p_1} \mathbf{E}; \mathbf{X}_{p_2} \mathbf{E}; \dots; \mathbf{X}_{p_N} \mathbf{E}], \quad \mathbf{Z}_0 \in \mathbb{R}^{N \times D}, \quad (2)$$

where \mathbf{Z}_0 represents the sequence of patch embeddings. Note that this process can be implemented utilizing a single convolution layer with a $P \times P$ kernel, C input channels, and D output channels. Class token \mathbf{X}_{cls} , an additional learnable embedding, is prepended to the sequence. Finally, position embeddings are added to retain positional information.

$$\mathbf{Z}' = [\mathbf{X}_{\text{cls}}; \mathbf{Z}_0] + \mathbf{E}_{\text{pos}}, \quad \mathbf{Z}' \in \mathbb{R}^{(N+1) \times D}. \quad (3)$$

Here, \mathbf{E}_{pos} denotes the position embeddings, and the resulting \mathbf{Z}' serves as the input to the subsequent layers of the ViT architecture.

Architecture overview

The patch embedding layer transforms the input image into a sequence of embeddings that the self-attention mechanism of the Transformer can process. A straightforward way to handle the input data from different modalities is to utilize multiple patch embedding layers to convert data with different spectral wavelengths into embeddings with the same dimension⁴². Suppose that the input image \mathbf{X} of dimensions $\mathbb{R}^{C \times H \times W}$ can originate from various data modalities. Initially, images from different sources are standardized to height H and width W . Specifically, we consider five distinct modalities: Sentinel 1 data (\mathbf{X}_{s1}) with two SAR channels ($\mathbb{R}^{2 \times H \times W}$), Sentinel 2 data (\mathbf{X}_{s2}) with nine multispectral channels ($\mathbb{R}^{9 \times H \times W}$), Gaofen data (\mathbf{X}_g) with four multispectral channels ($\mathbb{R}^{4 \times H \times W}$), NAIP imagery (\mathbf{X}_{rgb}) with three RGB channels ($\mathbb{R}^{3 \times H \times W}$), and EnMAP data (\mathbf{X}_e) with 202 available hyperspectral channels ($\mathbb{R}^{202 \times H \times W}$). Note that, for the sake of simplicity, we omit the batch size for the denotation of tensors. OFA-Net⁴² proposes a simple and straightforward way to use individual patch embedding layers for each data modality. However, while practical, this method is not flexible enough when the number of bands of downstream tasks changes.

In this context, inspired by the brain’s neuroplasticity, we propose a dynamic architecture to flexibly adapt the model to different modalities and handle variations in the number of spectral bands, as illustrated in Fig. 4a. The whole architecture follows the design of masked image modeling (MIM)⁴³. The main difference from

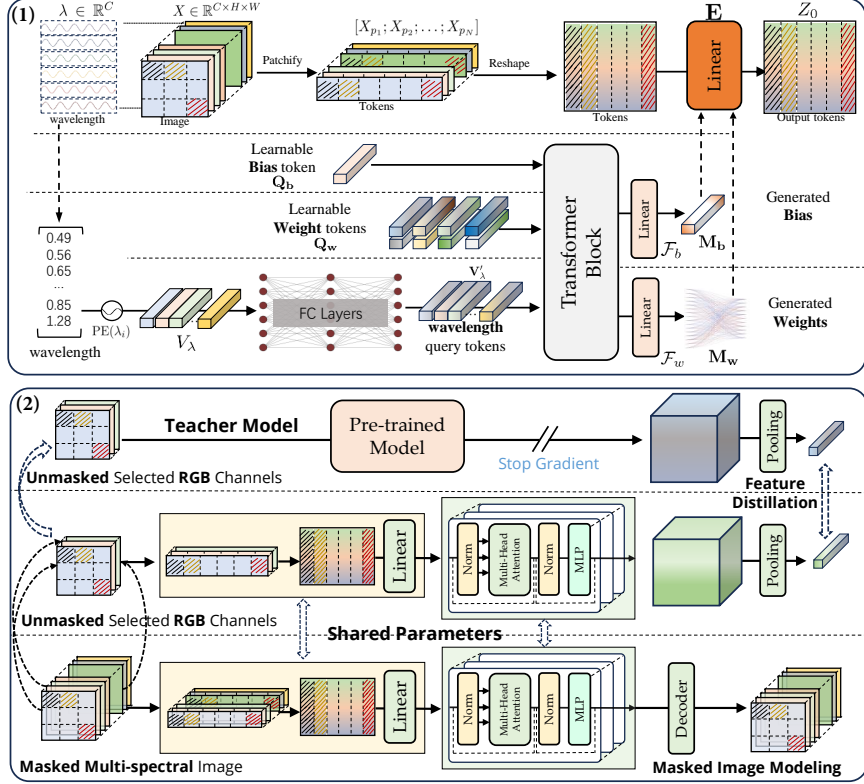
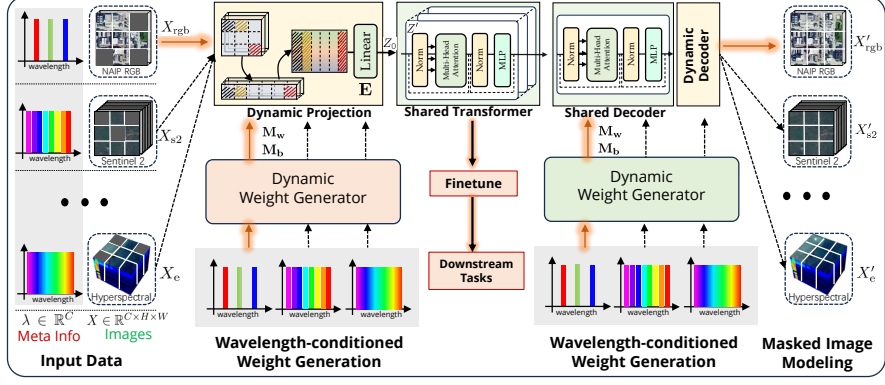


Fig. 4: (a) Architecture and training details. (a) Architecture design. DOFA builds on masked image modeling, introducing a significant advancement by processing input images with any number of channels within a single framework. **(b) Dynamic weight generator and continual training framework.** (1) The central wavelengths of each band are utilized to derive weights tailored to each wavelength. (2) Continual pretraining process. There is a distillation and a reconstruction loss.

traditional masked autoencoders (MAE) lies in DOFA’s capacity to process input images with various channels. This flexibility is achieved through a hypernetwork-based dynamic weight generator, a critical component of the model’s design. The dynamic weight generator takes inputs from the spectral wavelength associated with each image channel and predicts the patch embedding matrix \mathbf{E} for different data modalities dynamically to learn specific representations for each modality. The latent representations are then passed through a series of shared Transformer blocks for learning generalizable multimodal representations. These blocks apply self-attention mechanisms to capture the complex interactions between different image parts.

Parallel to the dynamic weight generation for the encoder part of the network, the dynamic decoder is responsible for reconstructing the output image from the encoded latent space. Similarly, the dynamic decoder utilizes another set of dynamically generated weights to ensure that the reconstructed image matches the number of spectral bands of the target modality. We employ a MIM strategy to train this self-supervised architecture. The input images are masked randomly, and the model learns to reconstruct these missing parts. As the parameters in DOFA are learned across different modalities, this process helps the model to learn robust multimodal representations beneficial for various EO tasks. After the pre-training process, the model can be fine-tuned for specific downstream tasks with fewer learnable parameters and training costs to tailor the model to specific EO applications without extensive retraining. The model can be transferred to various EO applications by integrating dynamic weight generation and decoding, from high-resolution optical imaging to multispectral and hyperspectral sensing.

Wavelength-conditioned dynamic patch embedding

To manage the diversity of spectral bands across different modalities, we project the data into a latent space with uniform feature dimensionality using the dynamic patch embedding layer \mathcal{F}_{dpe} . As described in the Mathematical formalism section, we denote the input image as $\mathbf{X} \in \mathbb{R}^{C \times H \times W}$. Fig. 4b (1) illustrates the detailed steps used to compute the dynamic weights given the wavelength information of each channel. Each channel of the input image has a corresponding central wavelength. The wavelengths of an input image with C channels can be represented by $\lambda \in \mathbb{R}^C$. To convert the wavelengths to a higher-dimensional feature space, we encode the wavelengths λ using a 1D sine-cosine positional encoding:

$$\mathbf{V}_\lambda = \text{PE}(\lambda) \in \mathbb{R}^{C \times D_\lambda}, \quad (4)$$

where D_λ is the dimension of the converted wavelength feature. The positional encoding $\text{PE}(\lambda_i)$ for wavelength λ_i in channel i is given by:

$$\begin{aligned} \text{PE}(\lambda_i, 2k) &= \sin\left(\frac{\lambda_i}{10000^{2k/D_\lambda}}\right), \\ \text{PE}(\lambda_i, 2k+1) &= \cos\left(\frac{\lambda_i}{10000^{2k/D_\lambda}}\right), \end{aligned} \quad (5)$$

where $k = 0, \dots, \frac{D_\lambda}{2} - 1$. The positionally encoded wavelengths \mathbf{V}_λ are further transformed through two fully-connected layers with residual connections:

$$\mathbf{V}'_\lambda = \text{ReLU}(\mathcal{F}_2(\text{ReLU}(\mathcal{F}_1(\mathbf{V}_\lambda)))) + \mathbf{V}_\lambda, \quad (6)$$

where \mathcal{F}_1 and \mathcal{F}_2 represent the fully-connected layers, and ReLU denotes the Rectified Linear Unit activation function⁴⁹.

Next, we employ a Transformer encoder⁵⁰ layer with four attention heads to generate the dynamic weights and bias for each wavelength. Specifically, the embedding \mathbf{V}'_λ , N_w learnable query tokens \mathbf{Q}_w , and one learnable bias query token \mathbf{Q}_b are concatenated together to form the input to the Transformer encoder:

$$\mathbf{V}'' = \text{TransformerEncoder}(\text{Concat}(\mathbf{Q}_w, \mathbf{V}'_\lambda, \mathbf{Q}_b)). \quad (7)$$

We subsequently extract the embeddings \mathbf{V}''_w that correspond to the weight query tokens \mathbf{Q}_w from \mathbf{V}'' , as well as the embeddings \mathbf{V}''_b associated with the bias query tokens \mathbf{Q}_b from \mathbf{V}'' . Then, two fully-connected layers are utilized to generate the dynamic weights and biases:

$$\begin{aligned} \mathbf{M}_w &= \mathcal{F}_w(\mathbf{V}''_w + \mathbf{V}'_\lambda) \in \mathbb{R}^{C \times P^2 D}, \\ \mathbf{M}_b &= \mathcal{F}_b(\mathbf{V}''_b) \in \mathbb{R}^{C \times D}, \end{aligned} \quad (8)$$

where \mathcal{F}_w and \mathcal{F}_b denote the fully-connected layers for weight and bias generation, respectively. As introduced in the Mathematical formalism section, the patch embedding layer can be implemented efficiently using a convolution layer. Thus, we reshape the generated weights into the convolution kernel as:

$$\mathbf{K}_{\text{conv}} = \text{Reshape}(\mathbf{M}_w, [D, C, P, P]), \quad (9)$$

The convolution operation for patch embedding is then performed using the dynamically generated weights \mathbf{K}_{conv} and biases \mathbf{M}_b :

$$\text{PatchEmbedding} := \text{Conv}(\mathbf{X}, \mathbf{K}_{\text{conv}}, \mathbf{M}_b). \quad (10)$$

where Conv denotes the convolution operation.

Utilizing this approach, the patch embedding layer achieves independence from the number of spectral bands of the input images. The weights for these layers are dynamically generated based on the central wavelength of each channel in a compositional manner. This mechanism enables the model to learn modality-specific representations dynamically, thereby enhancing its adaptability and performance across various data domains.

For the wavelength-conditioned dynamic decoder, we use different parameters to generate dynamic weights and biases. The computation process is similar to the dynamic patch embedding layer described before. In the vanilla masked autoencoder, the final layer of the decoder is usually implemented as a fully-connected layer to

convert features from latent space into pixel space. For the dynamic decoder layer, we follow the same process used in the dynamic patch embedding to generate the dynamic weights. The only difference is that a fully-connected layer is used in the decoder rather than the convolution layer in the patch embedding layer.

Multimodal continual pretraining

The self-supervised loss formulation is pivotal for training our multimodal EO foundation model. The model leverages the MIM paradigm to circumvent the necessity for spatially aligned multimodal datasets, which are challenging to construct. To reduce the computational cost of self-supervised training on extensive datasets, we design a continual pretraining strategy inspired by Mendieta et al. ²⁰ incorporating a distillation loss and a weight initialization strategy. This method effectively utilizes knowledge from expansive, supervised, pretrained models, reducing the computational burden and associated CO₂ emissions.

Given the disparities in spectral resolution between these datasets, using ImageNet pretrained weights for continual pretraining is challenging. Instead, we design a proxy-based distillation method that extracts optical data as a proxy to ensure representation similarity between the teacher and student networks. As illustrated in Fig. 4b (2), for multi-channel input data with more than three channels, we extract the RGB channels to form a three-channel input $\mathbf{X}_p \in \mathbb{R}^{3 \times H \times W}$. We randomly select one channel for Sentinel-1 data with only two bands and duplicate it to a synthetic three-channel image. This input \mathbf{X}_p is then fed into an ImageNet-pretrained teacher model to get teacher features \mathbf{F}_t . Concurrently, the dynamic encoder in DOFA is also used to encode \mathbf{X}_p into student features \mathbf{F}_s . Throughout this procedure, the teacher model’s weights remain frozen to preserve structured representations and reduce the computational load during optimization.

We also follow a continual pretraining strategy for initializing the dynamic weight generator. First, we pretrain the generator to mimic the teacher model’s patch embedding layer weights. We then use the pretrained weights to initialize the dynamic embedding layer.

The training loss comprises two distinct components. One is the MIM reconstruction loss, which forces the model to predict $\mathbf{X}' \in \mathbb{R}^{C \times H \times W}$ for reconstructing various data modalities from the full-channel inputs \mathbf{X} . The other is the feature distillation loss, which employs the cosine similarity between the teacher and student feature representations to guide the learning process of the student model. Suppose that the encoded feature of the full channel input is \mathbf{F} ; then the composite loss function can be formulated as follows:

$$\mathcal{L} = \frac{1}{N} \sum_{i=1}^N \|\mathbf{X}_i - \mathbf{X}'_i\|^2 - \frac{\mathcal{F}_P(\mathbf{F}_s^i) \cdot \mathbf{F}_t^i}{\|\mathcal{F}_p(\mathbf{F}_s^i)\|_2 \cdot \|\mathbf{F}_t^i\|_2}, \quad (11)$$

where \mathcal{F}_P is a linear projection layer, and N is the number of data samples. By employing this bifurcated loss function, our model’s training is supervised from two distinct perspectives. First, it leverages the complete spectral information present in the input to learn cross-modal features via image reconstruction. Second, it distills knowledge

from extensively pretrained models into diverse data modalities using a single, shared dynamic model. This approach enables efficient and robust feature learning and is adept at handling the complexities of various modalities.

Data availability

The curated datasets and pre-trained model weights will be available at <https://github.com/ShadowXZT/DOFA-pytorch> and <https://huggingface.co/XShadow/DOFA>.

Code availability

Code is available at <https://github.com/zhu-xlab/DOFA>.

References

- [1] Camps-Valls, G., Tuia, D., Gómez-Chova, L., Jiménez, S., Malo, J.: Remote sensing image processing (2011)
- [2] Camps-Valls, G., Tuia, D., Zhu, X.X., Reichstein, M.: Deep learning for the Earth sciences: A comprehensive approach to remote sensing, climate science and geosciences (2021)
- [3] Reichstein, M., Camps-Valls, G., Stevens, B., Jung, M., Denzler, J., Carvalhais, N., Prabhat: Deep learning and process understanding for data-driven Earth system science. *Nature* **566**(7743), 195–204 (2019)
- [4] Roy, D.P., Wulder, M.A., Loveland, T.R., Woodcock, C.E., Allen, R.G., Anderson, M.C., Helder, D., Irons, J.R., Johnson, D.M., Kennedy, R., *et al.*: Landsat-8: Science and product vision for terrestrial global change research. *Remote Sensing of Environment* **145**, 154–172 (2014)
- [5] Drusch, M., Del Bello, U., Carlier, S., Colin, O., Fernandez, V., Gascon, F., Hoersch, B., Isola, C., Laberinti, P., Martimort, P., *et al.*: Sentinel-2: ESA’s optical high-resolution mission for GMES operational services. *Remote Sensing of Environment* **120**, 25–36 (2012)
- [6] Salomonson, V.V., Barnes, W., Maymon, P.W., Montgomery, H.E., Ostrow, H.: MODIS: Advanced facility instrument for studies of the Earth as a system. *IEEE Transactions on Geoscience and Remote Sensing* **27**(2), 145–153 (1989)
- [7] Guanter, L., Kaufmann, H., Segl, K., Foerster, S., Rogass, C., Chabrillat, S., Kuester, T., Hollstein, A., Rossner, G., Chlebek, C., *et al.*: The EnMAP spaceborne imaging spectroscopy mission for Earth observation. *Remote Sensing* **7**(7), 8830–8857 (2015)

- [8] Huang, W., Sun, S., Jiang, H., Gao, C., Zong, X.: GF-2 satellite 1m/4m camera design and in-orbit commissioning. *Chinese Journal of Electronics* **27**(6), 1316–1321 (2018)
- [9] USDA Farm Service Agency (FSA): National Agriculture Imagery Program (NAIP). USDA Geospatial Data Gateway (2015)
- [10] Zhu, X.X., Tuia, D., Mou, L., Xia, G.-S., Zhang, L., Xu, F., Fraundorfer, F.: Deep learning in remote sensing: A comprehensive review and list of resources. *IEEE Geoscience and Remote Sensing Magazine* **5**(4), 8–36 (2017)
- [11] Schmitt, M., Ahmadi, S.A., Xu, Y., Taşkın, G., Verma, U., Sica, F., Hänsch, R.: There are no data like more data: Datasets for deep learning in Earth observation. *IEEE Geoscience and Remote Sensing Magazine* (2023)
- [12] Xiong, Z., Zhang, F., Wang, Y., Shi, Y., Zhu, X.X.: EarthNets: Empowering AI in Earth observation. arXiv preprint arXiv:2210.04936 (2022)
- [13] Bommasani, R., Hudson, D.A., Adeli, E., Altman, R., Arora, S., Arx, S., Bernstein, M.S., Bohg, J., Bosselut, A., Brunskill, E., et al.: On the opportunities and risks of foundation models. arXiv preprint arXiv:2108.07258 (2021)
- [14] Touvron, H., Lavril, T., Izacard, G., Martinet, X., Lachaux, M.-A., Lacroix, T., Rozière, B., Goyal, N., Hambro, E., Azhar, F., et al.: LLaMA: Open and efficient foundation language models. arXiv preprint arXiv:2302.13971 (2023)
- [15] Brown, T., Mann, B., Ryder, N., Subbiah, M., Kaplan, J.D., Dhariwal, P., Neelakantan, A., Shyam, P., Sastry, G., Askell, A., et al.: Language models are few-shot learners. *Advances in Neural Information Processing Systems* **33**, 1877–1901 (2020)
- [16] OpenAI: ChatGPT (June 26 version) [large language model] (2023). <https://chat.openai.com/chat>
- [17] Radford, A., Kim, J.W., Hallacy, C., Ramesh, A., Goh, G., Agarwal, S., Sastry, G., Askell, A., Mishkin, P., Clark, J., et al.: Learning transferable visual models from natural language supervision. In: *International Conference on Machine Learning*, pp. 8748–8763 (2021). PMLR
- [18] Li, J., Li, D., Xiong, C., Hoi, S.: BLIP: Bootstrapping language-image pre-training for unified vision-language understanding and generation. In: *International Conference on Machine Learning*, pp. 12888–12900 (2022). PMLR
- [19] Kirillov, A., Mintun, E., Ravi, N., Mao, H., Rolland, C., Gustafson, L., Xiao, T., Whitehead, S., Berg, A.C., Lo, W.-Y., et al.: Segment anything. arXiv preprint arXiv:2304.02643 (2023)

- [20] Mendieta, M., Han, B., Shi, X., Zhu, Y., Chen, C.: Towards geospatial foundation models via continual pretraining. In: Proceedings of the IEEE/CVF International Conference on Computer Vision, pp. 16806–16816 (2023)
- [21] Reed, C.J., Gupta, R., Li, S., Brockman, S., Funk, C., Clipp, B., Keutzer, K., Candido, S., Uyttendaele, M., Darrell, T.: Scale-MAE: A scale-aware masked autoencoder for multiscale geospatial representation learning. In: Proceedings of the IEEE/CVF International Conference on Computer Vision, pp. 4088–4099 (2023)
- [22] Tang, M., Cozma, A., Georgiou, K., Qi, H.: Cross-Scale MAE: A tale of multi-scale exploitation in remote sensing. *Advances in Neural Information Processing Systems* **36** (2024)
- [23] Wang, Y., Hernández, H.H., Albrecht, C.M., Zhu, X.X.: Feature guided masked autoencoder for self-supervised learning in remote sensing. arXiv preprint arXiv:2310.18653 (2023)
- [24] Cong, Y., Khanna, S., Meng, C., Liu, P., Rozi, E., He, Y., Burke, M., Lobell, D., Ermon, S.: SatMAE: Pre-training transformers for temporal and multi-spectral satellite imagery. *Advances in Neural Information Processing Systems* **35**, 197–211 (2022)
- [25] Stewart, A., Lehmann, N., Corley, I., Wang, Y., Chang, Y.-C., Ait Ali Braham, N.A., Sehgal, S., Robinson, C., Banerjee, A.: SSL4EO-L: Datasets and foundation models for Landsat imagery. *Advances in Neural Information Processing Systems* **36** (2024)
- [26] Fuller, A., Millard, K., Green, J.R.: CROMA: Remote sensing representations with contrastive radar-optical masked autoencoders. arXiv preprint arXiv:2311.00566 (2023)
- [27] Wang, Y., Albrecht, C.M., Braham, N.A.A., Liu, C., Xiong, Z., Zhu, X.X.: DeCUR: decoupling common & unique representations for multimodal self-supervision. arXiv preprint arXiv:2309.05300 (2023)
- [28] Hong, D., Zhang, B., Li, X., Li, Y., Li, C., Yao, J., Yokoya, N., Li, H., Ghamisi, P., Jia, X., et al.: SpectralGPT: Spectral remote sensing foundation model. *IEEE Transactions on Pattern Analysis and Machine Intelligence* (2024)
- [29] Bastani, F., Wolters, P., Gupta, R., Ferdinando, J., Kembhavi, A.: SatlasPretrain: A large-scale dataset for remote sensing image understanding. In: Proceedings of the IEEE/CVF International Conference on Computer Vision, pp. 16772–16782 (2023)
- [30] Hebb, D.O.: *The organization of behavior: A neuropsychological theory* (2005)

- [31] Zucker, R.S., Regehr, W.G.: Short-term synaptic plasticity. *Annual Review of Physiology* **64**(1), 355–405 (2002)
- [32] Dan, Y., Poo, M.-m.: Spike timing-dependent plasticity of neural circuits. *Neuron* **44**(1), 23–30 (2004)
- [33] Pittenger, C., Duman, R.S.: Stress, depression, and neuroplasticity: A convergence of mechanisms. *Neuropsychopharmacology* **33**(1), 88–109 (2008)
- [34] Dayan, E., Cohen, L.G.: Neuroplasticity subserving motor skill learning. *Neuron* **72**(3), 443–454 (2011)
- [35] Buckmaster, P.S., Zhang, G.F., Yamawaki, R.: Axon sprouting in a model of temporal lobe epilepsy creates a predominantly excitatory feedback circuit. *Journal of Neuroscience* **22**(15), 6650–6658 (2002)
- [36] Duman, C.H., Duman, R.S.: Spine synapse remodeling in the pathophysiology and treatment of depression. *Neuroscience Letters* **601**, 20–29 (2015)
- [37] Lillicrap, T.P., Santoro, A., Marris, L., Akerman, C.J., Hinton, G.: Backpropagation and the brain. *Nature Reviews Neuroscience* **21**(6), 335–346 (2020)
- [38] Zhang, T., Cheng, X., Jia, S., Li, C.T., Poo, M.-m., Xu, B.: A brain-inspired algorithm that mitigates catastrophic forgetting of artificial and spiking neural networks with low computational cost. *Science Advances* **9**(34), 2947 (2023)
- [39] Ha, D., Dai, A.M., Le, Q.V.: Hypernetworks. In: *ICLR 2017* (2017)
- [40] Deng, J., Dong, W., Socher, R., Li, L.-J., Li, K., Fei-Fei, L.: ImageNet: A large-scale hierarchical image database. In: *2009 IEEE Conference on Computer Vision and Pattern Recognition*, pp. 248–255 (2009). Ieee
- [41] Lacoste, A., Lehmann, N., Rodriguez, P., Sherwin, E.D., Kerner, H., Lütjens, B., Irvin, J.A., Dao, D., Alemohammad, H., Drouin, A., et al.: GEO-Bench: Toward foundation models for Earth monitoring. *arXiv preprint arXiv:2306.03831* (2023)
- [42] Xiong, Z., Wang, Y., Zhang, F., Zhu, X.X.: One for all: Toward unified foundation models for Earth vision. *arXiv preprint arXiv:2401.07527* (2024)
- [43] He, K., Chen, X., Xie, S., Li, Y., Dollár, P., Girshick, R.: Masked autoencoders are scalable vision learners. In: *Proceedings of the IEEE/CVF Conference on Computer Vision and Pattern Recognition*, pp. 16000–16009 (2022)
- [44] Dosovitskiy, A., Beyer, L., Kolesnikov, A., Weissenborn, D., Zhai, X., Unterthiner, T., Dehghani, M., Minderer, M., Heigold, G., Gelly, S., et al.: An image is worth 16x16 words: Transformers for image recognition at scale. *arXiv preprint arXiv:2010.11929* (2020)

- [45] Liu, Z., Lin, Y., Cao, Y., Hu, H., Wei, Y., Zhang, Z., Lin, S., Guo, B.: Swin transformer: Hierarchical vision transformer using shifted windows. In: Proceedings of the IEEE/CVF International Conference on Computer Vision, pp. 10012–10022 (2021)
- [46] Liu, Z., Mao, H., Wu, C.-Y., Feichtenhofer, C., Darrell, T., Xie, S.: A ConvNet for the 2020s. In: Proceedings of the IEEE/CVF Conference on Computer Vision and Pattern Recognition, pp. 11976–11986 (2022)
- [47] Xiao, T., Liu, Y., Zhou, B., Jiang, Y., Sun, J.: Unified perceptual parsing for scene understanding. In: Proceedings of the European Conference on Computer Vision (ECCV), pp. 418–434 (2018)
- [48] Maaten, L., Hinton, G.: Visualizing data using t-SNE. *Journal of Machine Learning Research* **9**(11) (2008)
- [49] Agarap, A.F.: Deep learning using rectified linear units (ReLU). arXiv preprint arXiv:1803.08375 (2018)
- [50] Vaswani, A., Shazeer, N., Parmar, N., Uszkoreit, J., Jones, L., Gomez, A.N., Kaiser, L., Polosukhin, I.: Attention is all you need. *Advances in Neural Information Processing Systems* **30** (2017)
- [51] Gao, P., Ma, T., Li, H., Lin, Z., Dai, J., Qiao, Y.: Convmae: Masked convolution meets masked autoencoders. arXiv preprint arXiv:2205.03892 (2022)
- [52] Manas, O., Lacoste, A., Giró-i-Nieto, X., Vazquez, D., Rodriguez, P.: Seasonal contrast: Unsupervised pre-training from uncurated remote sensing data. In: Proceedings of the IEEE/CVF International Conference on Computer Vision, pp. 9414–9423 (2021)
- [53] Zhang, L., Xiang, T., Gong, S.: Learning a deep embedding model for zero-shot learning. In: Proceedings of the IEEE Conference on Computer Vision and Pattern Recognition, pp. 2021–2030 (2017)
- [54] Sung, F., Yang, Y., Zhang, L., Xiang, T., Torr, P.H., Hospedales, T.M.: Learning to compare: Relation network for few-shot learning. In: Proceedings of the IEEE Conference on Computer Vision and Pattern Recognition, pp. 1199–1208 (2018)
- [55] Xiong, Z., Li, H., Zhu, X.X.: Doubly deformable aggregation of covariance matrices for few-shot segmentation. In: European Conference on Computer Vision, pp. 133–150 (2022). Springer
- [56] Liu, H., Li, C., Wu, Q., Lee, Y.J.: Visual instruction tuning. *Advances in Neural Information Processing Systems* **36** (2024)
- [57] Grill, J.-B., Strub, F., Altché, F., Tallec, C., Richemond, P., Buchatskaya, E.,

- Doersch, C., Avila Pires, B., Guo, Z., Gheshlaghi Azar, M., *et al.*: Bootstrap your own latent: A new approach to self-supervised learning. *Advances in Neural Information Processing Systems* **33**, 21271–21284 (2020)
- [58] Caron, M., Touvron, H., Misra, I., Jégou, H., Mairal, J., Bojanowski, P., Joulin, A.: Emerging properties in self-supervised vision transformers. In: *Proceedings of the IEEE/CVF International Conference on Computer Vision*, pp. 9650–9660 (2021)
- [59] Chen, T., Kornblith, S., Norouzi, M., Hinton, G.: A simple framework for contrastive learning of visual representations. In: *International Conference on Machine Learning*, pp. 1597–1607 (2020). PMLR
- [60] Frome, A., Corrado, G.S., Shlens, J., Bengio, S., Dean, J., Ranzato, M., Mikolov, T.: DeViSE: A deep visual-semantic embedding model. *Advances in Neural Information Processing Systems* **26** (2013)
- [61] Ye, L., Rochan, M., Liu, Z., Wang, Y.: Cross-modal self-attention network for referring image segmentation. In: *Proceedings of the IEEE/CVF Conference on Computer Vision and Pattern Recognition*, pp. 10502–10511 (2019)
- [62] Rombach, R., Blattmann, A., Lorenz, D., Esser, P., Ommer, B.: High-resolution image synthesis with latent diffusion models (2021)
- [63] Lu, J., Clark, C., Zellers, R., Mottaghi, R., Kembhavi, A.: Unified-IO: A unified model for vision, language, and multi-modal tasks. *arXiv preprint arXiv:2206.08916* (2022)
- [64] Zou, X., Dou, Z.-Y., Yang, J., Gan, Z., Li, L., Li, C., Dai, X., Behl, H., Wang, J., Yuan, L., *et al.*: Generalized decoding for pixel, image, and language. In: *Proceedings of the IEEE/CVF Conference on Computer Vision and Pattern Recognition*, pp. 15116–15127 (2023)
- [65] Zhang, Y., Gong, K., Zhang, K., Li, H., Qiao, Y., Ouyang, W., Yue, X.: Meta-transformer: A unified framework for multimodal learning. *arXiv preprint arXiv:2307.10802* (2023)
- [66] Mall, U., Hariharan, B., Bala, K.: Change-aware sampling and contrastive learning for satellite images. In: *Proceedings of the IEEE/CVF Conference on Computer Vision and Pattern Recognition*, pp. 5261–5270 (2023)
- [67] Cha, K., Seo, J., Lee, T.: A billion-scale foundation model for remote sensing images. *arXiv preprint arXiv:2304.05215* (2023)
- [68] Yao, F., Lu, W., Yang, H., Xu, L., Liu, C., Hu, L., Yu, H., Liu, N., Deng, C., Tang, D., *et al.*: RingMo-sense: Remote sensing foundation model for spatiotemporal prediction via spatiotemporal evolution disentangling. *IEEE Transactions*

on Geoscience and Remote Sensing (2023)

- [69] Irvin, J., Tao, L., Zhou, J., Ma, Y., Nashold, L., Liu, B., Ng, A.Y.: USat: A unified self-supervised encoder for multi-sensor satellite imagery. arXiv preprint arXiv:2312.02199 (2023)
- [70] Wang, Y., Braham, N.A.A., Xiong, Z., Liu, C., Albrecht, C.M., Zhu, X.X.: SSL4EO-S12: A large-scale multimodal, multitemporal dataset for self-supervised learning in Earth observation. *IEEE Geoscience and Remote Sensing Magazine* **11**(3), 98–106 (2023)
- [71] Ayush, K., Uzkent, B., Meng, C., Tanmay, K., Burke, M., Lobell, D., Ermon, S.: Geography-aware self-supervised learning. In: *Proceedings of the IEEE/CVF International Conference on Computer Vision*, pp. 10181–10190 (2021)
- [72] Cepeda, V.V., Nayak, G.K., Shah, M.: GeoCLIP: Clip-inspired alignment between locations and images for effective worldwide geo-localization. arXiv preprint arXiv:2309.16020 (2023)
- [73] Klemmer, K., Rolf, E., Robinson, C., Mackey, L., Rußwurm, M.: SatCLIP: Global, general-purpose location embeddings with satellite imagery. arXiv preprint arXiv:2311.17179 (2023)
- [74] Guo, X., Lao, J., Dang, B., Zhang, Y., Yu, L., Ru, L., Zhong, L., Huang, Z., Wu, K., Hu, D., et al.: SkySense: A multi-modal remote sensing foundation model towards universal interpretation for Earth observation imagery. arXiv preprint arXiv:2312.10115 (2023)
- [75] Jean, N., Wang, S., Samar, A., Azzari, G., Lobell, D., Ermon, S.: Tile2Vec: Unsupervised representation learning for spatially distributed data. In: *Proceedings of the AAAI Conference on Artificial Intelligence*, vol. 33, pp. 3967–3974 (2019)
- [76] Christie, G., Fendley, N., Wilson, J., Mukherjee, R.: Functional map of the world. In: *Proceedings of the IEEE Conference on Computer Vision and Pattern Recognition*, pp. 6172–6180 (2018)
- [77] Wang, Y., Braham, N.A.A., Xiong, Z., Liu, C., Albrecht, C.M., Zhu, X.X.: SSL4EO-S12: A large-scale multi-modal, multi-temporal dataset for self-supervised learning in Earth observation. arXiv preprint arXiv:2211.07044 (2022)
- [78] Tong, X.-Y., Xia, G.-S., Zhu, X.X.: Enabling country-scale land cover mapping with meter-resolution satellite imagery. *ISPRS Journal of Photogrammetry and Remote Sensing* **196**, 178–196 (2023)
- [79] Fuchs, M.H.P., Demir, B.: HySpecNet-11k: A large-scale hyperspectral dataset for benchmarking learning-based hyperspectral image compression methods. arXiv preprint arXiv:2306.00385 (2023)

- [80] Steiner, A., Kolesnikov, A., Zhai, X., Wightman, R., Uszkoreit, J., Beyer, L.: How to train your ViT? data, augmentation, and regularization in vision transformers. arXiv preprint arXiv:2106.10270 (2021)
- [81] Loshchilov, I., Hutter, F.: Decoupled weight decay regularization. arXiv preprint arXiv:1711.05101 (2017)
- [82] Cheng, G., Han, J., Lu, X.: Remote sensing image scene classification: Benchmark and state of the art. *Proceedings of the IEEE* **105**(10), 1865–1883 (2017)
- [83] Stewart, A.J., Robinson, C., Corley, I.A., Ortiz, A., Lavista Ferres, J.M., Banerjee, A.: TorchGeo: Deep learning with geospatial data. In: *Proceedings of the 30th International Conference on Advances in Geographic Information Systems. SIGSPATIAL '22*, pp. 1–12. Association for Computing Machinery, Seattle, Washington (2022). <https://doi.org/10.1145/3557915.3560953>

Acknowledgments

The work of Z.X., F.Z., Y.W., F.Z., A.J.S., and X.X.Z is jointly supported by the German Federal Ministry of Education and Research (BMBF) in the framework of the international future AI lab “AI4EO – Artificial Intelligence for Earth Observation: Reasoning, Uncertainties, Ethics and Beyond” (grant number: 01DD20001), by German Federal Ministry for Economic Affairs and Climate Action in the framework of the “national center of excellence ML4Earth” (grant number: 50EE2201C), by the German Federal Ministry for the Environment, Nature Conservation, Nuclear Safety and Consumer Protection (BMUV) based on a resolution of the German Bundestag (grant number: 67KI32002B; Acronym: *EKAPEX*) and by Munich Center for Machine Learning. The work of Z. X., I.P., G.C.V., and X. X. Z is also funded by the European Commission through the project “ThinkingEarth—Copernicus Foundation Models for a Thinking Earth” under the Horizon 2020 Research and Innovation program (Grant Agreement No. 101130544). GCV was partly funded by the European Research Council (ERC) Synergy Grant “Understanding and Modeling the Earth System with Machine Learning” (USMILE) under the Horizon 2020 Research and Innovation program (Grant Agreement No. 855187).

Extended Data Table 1: Classification results on the RESISC-45 dataset. The best results are shown in bold.

Methods	Backbone	Frozen	Finetune
Scale-MAE ²¹	Vit-Large	89.6	95.7
SatMAE ²⁴	Vit-Large	88.3	94.8
ConvMAE ⁵¹	ConvVit-Large	81.2	95.0
Vanilla MAE ⁴³	Vit-Large	88.9	93.3
DOFA	Vit-Base	91.3	97.3
DOFA	Vit-Large	91.9	97.8

Extended Data Table 2: Segmentation results on the Seg-Munich dataset. The mean intersection over union (mIoU) is reported, and the best results are shown in bold.

Method	Pretrained Dataset	mAcc	mIoU
ResNet50	ImageNet-1k	80.1	45.6
SeCo ⁵²	SeCo	80.3	45.9
ViT (Random init.) ⁴⁴	-	81.0	47.3
ViT-22k ⁴⁴	ImageNet-22k	81.7	48.3
SatMAE ²⁴	fMoW-S2	81.5	48.7
SpectralGPT ²⁸	fMoW-S2	82.5	49.8
SpectralGPT+ ²⁸	fMoW-S2+BigEarthNet	82.7	51.0
DOFA (ViT-Base)	DOFA Multimodal Dataset	83.4	51.6

Supplementary materials

A. Related methods

Recently, foundation models¹³ have showcased remarkable success in transferring to a broad range of downstream tasks within a unified paradigm. These transfer learning techniques include fine-tuning, zero-shot⁵³, or few-shot^{54,55} learning, as well as instruction tuning⁵⁶. One of the critical factors that contribute to the success of foundation models is self-supervised learning, with typical methods including BYOL⁵⁷, DINO⁵⁸, and MAEs⁴³. These methods harness techniques like contrastive learning⁵⁹ and next token prediction to enable the exploration of large-scale data without human annotation.

Real-world data are characterized by diverse modalities, including but not limited to images, videos, text, audio, depth information, and point clouds. The capacity of foundation models to effectively handle this variety of downstream tasks hinges on their ability to process multimodal data. In this context, visual-language foundation models have emerged as a preceding and significant area of research. These models are adept at developing a universal representation that seamlessly merges visual and language modalities. Their work encompasses a broad spectrum of visual-language understanding¹⁷ tasks, addressing different levels of granularity and facilitating various cross-modal reasoning applications like image-text retrieval⁶⁰ and image referring⁶¹. Additionally, they extensively explore a wide range of text-based visual generation⁶² tasks.

A critical research question in developing multimodal foundation models is how a unified representation for various input modalities and output formats can be achieved. Approaches capable of achieving such a representation are often referred to as unified frameworks^{63,64}. A notable example is the Meta-Transformer⁶⁵, which first employs a data-to-sequence tokenizer to convert data from 12 different modalities into a shared embedding space and subsequently trains a shared encoder to generate the unified multimodal representation.

In EO, the necessity of a unified multimodal foundation model becomes increasingly significant. In contrast to natural scene images, EO data typically manifests diverse characteristics. It can be captured by various sensors such as Landsat, Sentinel, MODIS, EnMAP, and NAIP, which feature varying numbers of spectral bands, spatial resolutions, and temporal repeat periods. Despite these differences, the data from these sources often exhibit distinct yet related characteristics. For instance, optical, multispectral, and hyperspectral images may share similar attributes in bands with similar wavelengths. EO data with similar ground sampling distance (GSD) may exhibit higher similarity. This underscores the imperative for a more sophisticated approach to multimodal representation learning for EO data.

Early efforts to develop EO foundation models were devoted to generating effective embeddings for data from a single modality. Examples include SeCo⁵² and CACo⁶⁶, which leverage temporal information from acquired images to learn temporal-sensitive and temporal-invariant feature representations. GFM²⁰ devises a continual pretraining paradigm that leverages ImageNet pretrained features to accelerate model convergence on EO data. Cha et al.⁶⁷ explore the impact of scaling up the number of parameters

in foundation models, specifically on Google Earth images. Another line of research addresses the adaptability of feature representations across EO data with different GSD. RingMo⁶⁸ introduces a patch-incomplete mask strategy during the masked image modeling phase, preventing the oversight of small objects within a single patch. Scale-MAE²¹ takes a different approach by substituting the positional encoding within ViT⁴⁴ with a GSD positional encoding, incorporating GSD information into the representation learning process. USat⁶⁹ adopts a strategy of encoding a higher number of patches for bands with lower GSD and a lower number of patches for bands with higher GSD. Another significant research question is how to achieve a unified representation for different modalities, such as RGB, multispectral, hyperspectral, and radar data. In this regard, SSL4EO-S12⁷⁰ integrates the features from multispectral and SAR modalities using an early fusion strategy.

SatMAE²⁴ suggests grouping subsets of spectral bands and adding a spectral encoding to each spectral group. CROMA²⁶ first develops two unimodal encoders to encode multispectral and SAR data individually. Subsequently, it utilizes a cross-modal radar-optical transformer that leverages cross-attention to extract the unified representation. DeCUR²⁷ is a bi-modal self-supervised foundation model that decouples the unique and common representations between the two modalities. SpectralGPT²⁸ is a foundation model meticulously tailored for hyperspectral remote sensing data. It designs a 3D masking strategy, an encoder for learning representations from spatial-spectral mixed tokens, and a decoder with multi-target reconstruction to preserve spectral characteristics. Beyond these, efforts have also been directed towards encoding geo-locational information into the feature representation. Notable examples include GASSL⁷¹, GeoCLIP⁷², SatCLIP⁷³, SkySense⁷⁴ and Tile2Vec⁷⁵. However, existing models cannot process data from a wide variety of EO sensors and cannot handle situations where the number of spectral bands changes in downstream tasks. DOFA overcomes this by employing a dynamic weight generator to encode spectral bands into dynamic weights for deep representation learning.

B. Models

More detailed information about the compared models is provided as follows:

1. rand. init. denotes the ViT model that is randomly initialized without using any pretrained weights.
2. MAE.Single denotes the vanilla MAE⁴³ model that is trained on the five individual modalities (as shown in Fig. S1).
3. OFA-Net⁴² is trained on the five modalities using different patch embedding layers. A shared Transformer backbone learns common representations from the multimodal EO data. OFANet is pretrained on a subset (50,000 samples) of the curated multimodal dataset for **100 epochs**.
4. SatMAE²⁴ proposes to group channels into subsets and add a spectral encoding to each spectral group. Specifically, we use the weights pretrained for **200 epochs** on the fMoW⁷⁶ dataset. The model processes Sentinel-2 data with ten bands, which are split into three groups (0, 1, 2, 6), (3, 4, 5, 7), (8, 9).

5. Scale-MAE²¹ contributes by introducing a scale-aware positional encoding strategy and a multi-scale decoder-based MAE framework. This method significantly enhances self-supervised learning performance. Scale-MAE is pretrained on the fMoW-RGB⁷⁶ dataset with a ViT-Large backbone for **800 epochs**. We use the provided pretrained weights for the transfer learning experiments.
6. GFM²⁰ proposes a continual pretraining method for training remote sensing foundation models. For GFM, a Swin-Base backbone is pretrained on the curated GeoPile dataset (600k images) for **100 epochs**. We use the provided pretrained weights for the transfer learning experiments.
7. Cross-Scale MAE²² designs a cross-scale MAE by enforcing cross-scale information consistency at both structural and semantic levels. A ViT-Base backbone is pretrained for **400 epochs** on the fMoW-RGB⁷⁶ dataset. We use the provided pretrained weights for the transfer learning experiments.
8. CROMA²⁶ combines contrastive and reconstruction self-supervised objectives to learn rich unimodal and multimodal representations. A ViT-base backbone is pretrained for **300 epochs** on the SSL4EO-S12⁷⁷ dataset. We use the provided pretrained weights for the transfer learning experiments.
9. FG-MAE²³ proposes to reconstruct a combination of Histograms of Oriented Gradients (HOG) and Normalized Difference Indices (NDI) features for multispectral images and HOG for SAR images instead of raw pixels. FG-MAE is pretrained on the SSL4EO-S12⁷⁰ dataset for **100 epochs** with the ViT-base backbone.

C. Datasets

Pre-training Datasets

During the self-supervised learning phase, we pretrain our model on large-scale data collected from five distinct modalities. These modalities encompass RGB aerial images from the National Agriculture Imagery Program (NAIP), multispectral (RGB + infrared) images from Gaofen-2, multispectral images from Sentinel-2, SAR images (VV and VH polarization) from Sentinel-1, and hyperspectral images from EnMAP.

As shown in Fig. S1, we have constructed an extensive multimodal dataset to underpin the development of unified foundation models for Earth vision. This dataset is composed of five distinct modalities, each offering unique spectral and spatial data characteristics:

Sentinel-1

The Sentinel-1 subset includes 4,642,353 samples of Synthetic Aperture Radar (SAR) imagery, with a spatial resolution of about 5×20 m. For Sentinel-1 data, we use the data collected in the SatalasPretrain dataset²⁹. Each image captures two bands (VV and VH) and is 512×512 pixels, providing dense global coverage.

Sentinel-2

We use the Sentinel-2 data collected and processed by Bastani et al.²⁹. The Sentinel-2 subset comprises 977,774 multispectral imagery samples, each with a spectral range

of nine bands, from 0.49 to 2.15 μm , maintaining a spatial resolution of 10 m, with each image sized at 512×512 pixels for dense global coverage.

Gaofen

To include images from the Gaofen satellite, we use the dataset collected by Tong et al.⁷⁸. This dataset mainly covers different cities in China. We crop 117,450 image patches of 512×512 pixel resolution from the dataset. In this dataset, each image includes four bands encompassing RGB and NIR wavelengths with a spatial resolution of around 4 m.

NAIP

For high-resolution optical images, we use the dataset collected and processed by Bastani et al.²⁹. This dataset includes 2,332,351 high-resolution aerial images from the National Agriculture Imagery Program (NAIP), covering the USA with a fine spatial resolution of approximately 1 m and consisting of RGB images across three bands with a size of 512×512 pixels.

EnMAP

The multimodal dataset for pretraining is further enriched with 11,483 hyperspectral image samples from EnMAP. We use the hyperspectral dataset published by Fuchs and Demir⁷⁹. The hyperspectral images have a spatial resolution of 30 m and capture a wide spectral range with 224 bands, each sized at 128×128 pixels.






Curated Datasets from Different Sensors				
 Sentinel 1	#Samples: 4,642,353	Size: 512x512	Coverage: Global (Dense)	Sensor: Sentinel 1 Geotag: Yes Wavelength: Microwave (2 bands) Capture time: Yes GSD: 20 m
 Sentinel 2	#Samples: 977,774	Size: 512x512	Coverage: Global (Dense)	Sensor: Sentinel 2 Geotag: Yes Wavelength: 0.49 ~ 2.15 (9 bands) Capture time: Yes GSD: 20 m
 Gaofen	#Samples: 117,450	Size: 512x512	Coverage: China	Sensor: Gaofen Geotag: Yes Wavelength: RGB, NIR (4 bands) Capture time: Yes GSD: 4 m
 Aerial Images	#Samples: 2,332,351	Size: 512x512	Coverage: USA	Sensor: Aerial Image Geotag: Yes Wavelength: RGB (3 bands) Capture time: Yes GSD: 1 m
 EnMAP	#Samples: 11,483	Size: 128x128	Coverage: Global (Sparse)	Sensor: EnMAP Geotag: Yes Wavelength: 0.46~2.45 (224 bands) Capture time: Yes GSD: 30 m

Fig. S1: The curated multimodal dataset. Five data modalities with different spatial resolutions and spectral bands are included: the data from Sentinel 1, Sentinel 2, Gaofen, aerial images, and the EnMAP mission.

Downstream task datasets

We evaluate the pretrained models on 12 downstream tasks organized in GEO-Bench⁴¹. These datasets cover various applications and data modalities in EO, including six classification tasks and six segmentation tasks. In addition, we also compare DOFA with existing state-of-the-art models on the RESISC-45 and SegMunich datasets to evaluate the effectiveness of our model.

Classification datasets

m-bigearthnet is a multi-label land cover land use classification dataset covering Europe. The dataset contains 22,000 Sentinel-2 images with patch size 120×120 pixels. Each image belongs to one or more categories from 43 classes.

m-so2sat is a local climate zone classification dataset. The dataset contains 21,964 Sentinel-1 and Sentinel-2 image pairs, covering 42 cities around the globe. Each image has a patch size of 32×32 and belongs to one of 17 types of local climate zones.

m-brick-kiln is a binary scene classification dataset to detect brick kilns, a highly polluting informal industry common in Bangladesh. It contains 17,061 Sentinel-2 images, each with a patch size of 64×64 .

m-forestnet is a dataset for classifying the drivers of primary forest loss in Indonesia. The dataset contains 8,446 Landsat-8 images of size 332×332 , distributed into 12 classes.

m-eurosat is an EU-wide land cover land use classification dataset. It contains 4,000 Sentinel-2 images with a size of 64×64 and includes ten land cover land use classes.

m-pv4ger is a dataset for detecting solar panels. It has both classification and segmentation versions. The classification version is a binary classification task with 13,812 high-resolution RGB images of size 320×320 pixels and resolution 0.1 m.

Segmentation tasks

m-pv4ger-seg is the segmentation version of the m-pv4ger dataset for solar panel detection. It contains 3,806 high-resolution RGB images with size 320×320 pixels.

m-chesapeake-landcover is a high-resolution land cover mapping dataset covering the contiguous US, with seven land cover classes. The dataset contains 5,000 RGB-NIR images with 1 m resolution and 256×256 pixels patch size.

m-cashew-plantation is a cashew mapping dataset covering a 120 km^2 area in Benin to characterize the expansion of cashew plantations. It contains 1,800 Sentinel-2 images with patch size 256×256 pixels.

m-SA-crop-type is a dataset for crop type segmentation from Sentinel-2 images. It contains 5,000 256×256 pixels images covering an area in Brandenburg, Germany, and an area in Western Cape, South Africa.

m-nz-cattle is a binary cow detection dataset from high-resolution aerial images. It contains 655 0.1 m resolution RGB images, each with size 500×500 .

m-NeonTree is a dataset for canopy crown detection and delineation in co-registered airborne RGB, LiDAR, and hyperspectral images. It contains 457 multimodal image pairs with size 400×400 and resolution 0.1 m.

D. Training

Pretraining

In the proposed DOFA, we use the central wavelengths of each spectral band as input to the dynamic weight generator. We convert the wavelength values uniformly to micrometer units μm for each spectral band. For SAR images from Sentinel-1, the wavelength is uniquely larger than other bands, and therefore the μm unit is not reasonable. We thus set the λ to 3.75 to distinguish it from different bands.

We pretrain vision transformers (base and large) with patch size 16 on the collected multimodal pretraining dataset. We initiate pretraining for the baseline “MAE_Single” model using a subset of 50,000 images. For each of the five modalities, we randomly choose 10,000 samples. The DOFA models are pretrained progressively. Initially, we pretrained the DOFA models on the subset containing 50,000 images for 100 epochs. Subsequently, we further pretrained the models on an expanded set of 410,000 images over 20 epochs. During this phase, we select 100,000 samples from each of the Sentinel-1, Sentinel-2, Gaofen, and NAIP modalities. For hyperspectral images, we choose 10,000 samples from EnMAP data. Finally, we conduct a single epoch on the entire curated dataset to complete the training. We randomly crop and resize each image to 224×224 as the input size to the ViT encoders. We normalize the images based on each modality’s mean and standard deviation. For the teacher models, we use the models of ViT-Base and ViT-Large pretrained on the ImageNet21K⁸⁰.

We adopt the masked image modeling design of MAE⁴³ for self-supervised pretraining, which includes a regular ViT encoder and a lightweight ViT decoder. Only the encoder is transferred to downstream tasks. The masking ratio is set to 75%. We pretrain ViTs with a batch size of 128 for 100 epochs. We use the AdamW optimizer⁸¹ with a weight decay of 0.05 and an initial learning rate of $1.5e-4$. The learning rate is warmed up for 20 epochs and then decayed with a cosine schedule.

Transfer learning

We use the data loading tool of GEO-Bench⁴¹ to load the downstream datasets. We freeze the transferred encoder and train a linear classifier for classification tasks. Similarly, we freeze the encoder and train a UPerNet⁴⁷ decoder for segmentation tasks. For all the models except the GFM with Swin Transformer, we transform the features into a feature pyramid with channels 512 and four different scales: 4, 2, 1, 0.5. The UPerNet segmentation head is then used to output the segmentation results. More architecture details can be found in the code implementation.

We follow the common practice of using RandomResizedCrop (scale 0.8 to 1.0) and RandomHorizontalFlip as data augmentations for classification tasks. The default crop size is 224×224 for all datasets and baseline models except SatMAE²⁴ and CROMA²⁶, of which the crop size is 96×96 for SatMAE and 120×120 for CROMA following the official setup to match their smaller patch size of 8. We use center crop, random rotation, and random horizontal and vertical flips for segmentation tasks. Images of each dataset are normalized based on the dataset’s mean and standard deviation.

We optimize cross-entropy loss for most datasets except m-bigearthnet, for which the MultiLabelSoftMarginLoss (or binary cross-entropy loss) is used. The LARS optimizer is utilized with cosine decay to train the last linear layer of each foundation model for 50 epochs. Considering the wide range of diversity among existing foundation models, we employ dataset-specific learning rates and batch sizes tailored to enhance the performance of classification tasks. We sweep over a grid search to pick the best learning rate from [0.5, 1.0, 10, 20] for each dataset. We use the AdamW optimizer, batch size 64, and an initial learning rate of 0.005 with cosine decay for 20 epochs for segmentation tasks. The learning rate is relatively stable across datasets for segmentation tasks.

E. Additional results

We employ a radar chart to illustrate these models’ comparative performance across various datasets concisely. Fig. S2 (a) reveals that DOFA models achieve impressive performance across all six datasets, highlighting the model’s versatility and efficiency. Similarly, Fig. S2 (b) shows that DOFA demonstrates robust applicability across diverse downstream tasks.

We visualize the accuracy curves of different SOTA models in Fig. S3 for the classification and segmentation datasets. These figures show that the proposed DOFA converges faster than other models on different datasets. A lower fine-tuning loss on downstream tasks suggests a higher adaptability of the foundation model to the specific dataset.

Extended Data Table S1: Classification results on the RESISC-45 dataset.

Methods	Backbone	Frozen	Finetune
Scale-MAE ²¹	Vit-Large	89.6	95.7
SatMAE ²⁴	Vit-Large	88.3	94.8
ConvMAE ⁵¹	ConvVit-Large	81.2	95.0
Vanilla MAE ⁴³	Vit-Large	88.9	93.3
DOFA	Vit-Base	91.3	97.3
DOFA	Vit-Large	91.9	97.8

Full fine-tuning experimental settings

In addition to the datasets in GEO-Bench, we compare DOFA with existing foundation models on the widely-used RESISC-45 dataset⁸². These results are presented in Table S1. The linear probing (frozen) and full fine-tuning settings are used for performance comparison. The results are also shown in Table S1. For fully fine-tuning the RESISC-45 dataset, we train both models (ViT-Base and ViT-Large) for 100 epochs with a base learning rate of $4e-3$ and a weight decay of $5e-3$. Note that the learning rate on the backbone is multiplied by 0.1. We set the learning rate to 0.1 for the linear probing setting and the weight decay to 0.05. When the backbone is frozen, DOFA

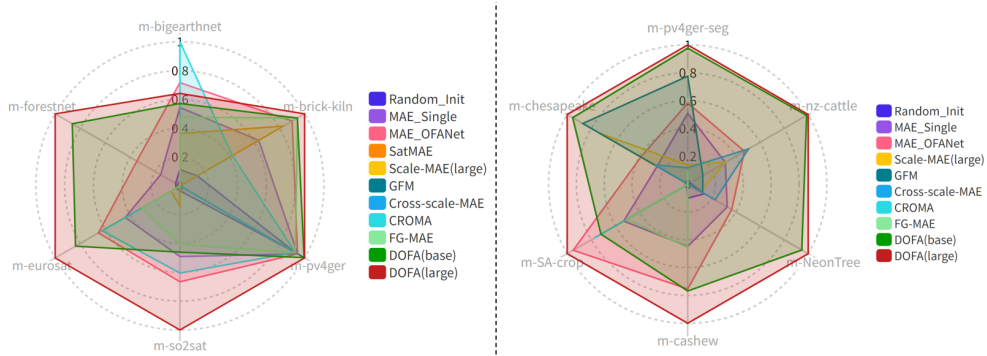


Fig. S2: Performance of different foundation models on GEO-Bench. DOFA, a single unified foundation model, can outperform most of the specifically trained SOTA foundation models on both classification (left side) and segmentation datasets (right side). These results demonstrate the effectiveness and versatility of DOFA. In the radar chart, min-max normalization is applied for clarity.

(ViT-Large) can achieve a top-1 overall accuracy of 91.9%, significantly better than other models. For the full fine-tuning results, DOFA also outperforms existing models by a large margin, demonstrating its effectiveness.

Extended Data Table S2: Segmentation results on the SegMunich dataset. The mean intersection over union (mIoU) is reported, and the best results are shown in bold.

Method	Pretrained Dataset	mAcc	mIoU
ResNet50	ImageNet-1k	80.1	45.6
SeCo ⁵²	SeCo	80.3	45.9
ViT (Random init.) ⁴⁴	-	81.0	47.3
ViT-22k ⁴⁴	ImageNet-22k	81.7	48.3
SatMAE ²⁴	fMoW-S2	81.5	48.7
SpectralGPT ²⁸	fMoW-S2	82.5	49.8
SpectralGPT+ ²⁸	fMoW-S2+BigEarthNet	82.7	51.0
DOFA (ViT-Base)	DOFA Multimodal Dataset	83.4	51.6

On the SegMunich dataset²⁸, we conduct full fine-tuning experiments to compare DOFA’s performance to recent state-of-the-art foundation models. SegMunich is a segmentation dataset that comprises 10-band Sentinel-2 data with a spatial resolution of 10 meters. This dataset covers the urban landscape of Munich and includes segmentation masks for 13 distinct Land Use and Land Cover (LULC) classes.

In our experimental setup, we utilize a batch size of 96 and a learning rate of 0.0005. The model is trained over 80,000 steps using UperNet as the segmentation head. Given that the patch size of DOFA is 16, we set the input image size to 256×256 to meet the higher resolution requirements of the segmentation task. We benchmark the DOFA model against seven other methodologies, establishing its capability to achieve

SOTA performance. Notably, while DOFA is designed as a versatile foundation model suitable for various data modalities, including SAR, hyperspectral, and multispectral images, it consistently outperforms foundation models that are tailored for a specific modality. Our results highlight DOFA’s exceptional adaptability and effectiveness, underscoring its potential as a robust, general-purpose model for Earth observation and remote sensing tasks.

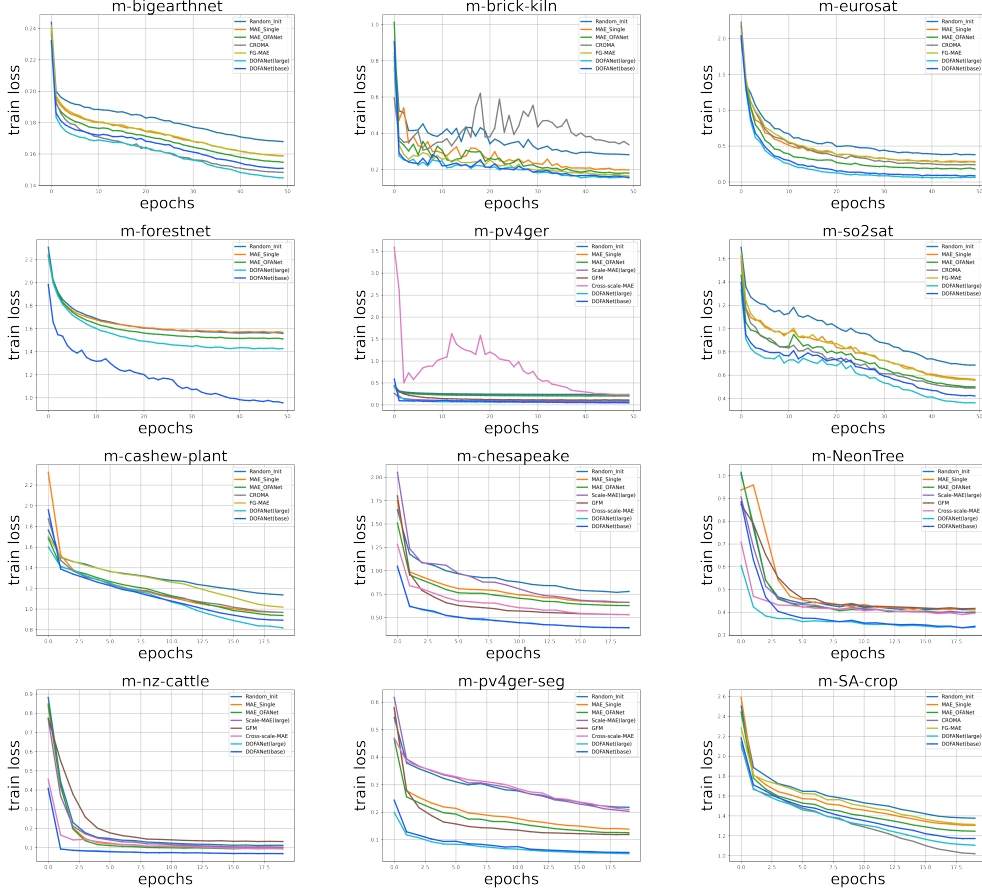


Fig. S3: Loss curves of different foundation models on the classification and segmentation datasets. It can be seen that the proposed DOFA converges faster than other models on these datasets.

F. Using the model and weights

The DOFA model and pre-trained weights are distributed via the TorchGeo library⁸³. The pre-trained model can be easily instantiated using the following code.

```
1 import torch
2 from torchgeo.models import DOFABase16_Weights, dofa_base_patch16_224
3
4 # Example NAIP image (wavelengths in micrometer)
5 x = torch.rand(2, 4, 224, 224)
6 wavelengths = [0.48, 0.56, 0.64, 0.81]
7
8 # Use pre-trained model weights
9 model = dofa_base_patch16_224(weights=DOFABase16_Weights.DOFA_MAE)
10
11 # Make a prediction (model may need to be finetuned first)
12 y = model(x, wavelengths)
```
